


paper 7

 [Composite Structures 247 \(2020\) 112474](https://doi.org/10.1016/j.compstruct.2020.112474)

Contents lists available at [ScienceDirect](https://www.sciencedirect.com)

Composite Structures

journal homepage: www.elsevier.com/locate/compstruct

 Experimental investigation on the dynamic behavior of 3D printed CF-PEKK composite under cyclic uniaxial compression M. Nachtane ^{a, *}, M. Tarfaoui ^b, Y. Ledoux ^a, S. Khammassi ^b, E. Leneveu ^c, J. Pelleter ^c

^aUniversity of Bordeaux, CNRS, Arts et Metiers Institute of Technology, Bordeaux INP, INRAE, I2M Bordeaux, F-33400 Talence, France ^bENSTA Bretagne, FRE CNRS 3744, IRDL, F-29200 Brest, France ^cNANOVIA, ZA Saint-Paul, 22540 Louargat, France

ARTICLE INFO

Keywords:

Additive manufacturing Dynamic behaviour Cyclic impact Infill effect SHPB

ABSTRACT

The main goal of the present work was to investigate the effect of infill density on dynamic behavior of 3D printed parts [Code a2]. The short carbon-fibre-reinforced PolyEtherKetoneKetone composites (CF-PEKK)

was selected as material which has an excellent mechanical, physical, thermal and energy absorbing performance. It's employed widely in a vast range of industries due to their ultra-low density, multi-functionality and ability to undergo large deformations at low loads [Code a3]. For this purpose, a procedure for characterizing the dynamic behavior of this material fabricated with Fused Filament Fabrication (FFF) is presented in this research. Three infill densities (20%, 50% and 100%) were experimentally compressed for different impact pressures (1,4 bar; 1,7 bar; 2 bar and 2,4 bar) using Split Hopkinson Pressure Bar (SHPB). A FASTCAM high-speed camera was positioned in front of the SHPB test set-up to capture the dynamic deformation processes. The special attention is also given to examine the dynamic response of 3D printed CF-PEKK (100% infill density) subjected to repeated impacts [Code a3]. The obtained results proved that the low density and high-density infills were more cost-effective when compared to solid samples [Code a5]. The repeated impact drastically changed the dynamic behavior of the material compared to standard impact [Code a4]. With increasing the number of impact loading to the final failure, the dynamic parameters (i.e dynamic modulus, maximum stress...etc.) decreased remarkably and the material suffered catastrophic cumulated damage. [Code a5]

1. Introduction

The development of civilization obliges researchers and engineers to find the new solutions and technologies requisite to optimize the manufacturing process of the product in all human activities. Traditionally, the composite materials are fabricated using the injection molding or in the case of honeycombs, using extrusion or welding [1]. In this context, additive manufacturing (AM) is a breakthrough technology that is changing the way products are made. The AM revolution stems from several benefits over traditional manufacturing processes such as mass customization; complex designs and geometries; waste reduction; supply chain simplification; faster time-to-market; drastic assembly reduction; reduction of weight (topology optimization) and low volume manufacturing [2].

Since there are no much works on the study of the dynamic behavior of honeycomb composites manufactured by 3D printing at the high-strain rate. Through this work, one wishes to show the mechanical performance of CF-PEKK subjected to dynamic loading and * Corresponding author.

E-mail address: mourad.nachtane@u-bordeaux.fr (M. Nachtane).

repeated impact to find a compromise between weight, resistance and shock absorption. In general, the mechanical performance of honeycombs structures depends on the solid of which they are made from, cell geometry, relative density and several factors such as manufacturing process characteristics, structural boundary and loading conditions [3–7]. According to the literature, several papers have been published on the study of the static and dynamic behaviour of honeycomb fabricated by additive manufacturing. Several researchers have worked on the effects of the infill density and print orientation on the mechanical performance of end products[8,9]. Yang et al.[3]studied the mechanical properties of 3D re-entrant honeycomb auxetic structures realized via additive manufacturing. Fadida et al.[10]studied the mechanical properties of Ti6Al4V specimens fabricated by additively manufactured (AM) under static and dynamic compression. The results indicated that the laser prepared dense material expose an excellent resistance compared to the same traditional material subjected to dynamic and static loads, but the ductility of the two was comparable. Tsouknidas et al. [11] Investigated the impact absorption of PLA sam-

<https://doi.org/10.1016/j.compstruct.2020.112474>

Received 28 February 2020; Revised 2 May 2020; Accepted 14 May 2020

Available online 16 May 2020

02638223/© 2020 Elsevier Ltd. All rights reserved.

ples printed by additive manufacturing with different printing speeds. The PLA samples were subjected to the compression load. The study has shown that the lowest printing speed given the highest tensile strength. Fernandez et al. [12] studied the influence of infill density on the tensile mechanical response in desktop 3D printing. Wyatt et al. [13] studied the nonlinear scaling effects in the stiffness of soft cellular structures. The results showed a good correlation between the finite element simulation and experimental results. Zhang et al.

[14] proved that a honeycombs structure fabricated by additive manufacturing from polycaprolactone can recuperate by 80% after a single compression to densification.

Recently, Antolak-Dudka et al. [15] studied the static and dynamic behaviour of honeycomb structures Ti6Al4V fabricated by Laser Engineered Net Shaping (LENSTM) in order to evaluate its ability to absorb impact energy. Simon and his colleagues [16] conducted an experimental investigation to understand the compressive behaviour of 3D printed thermoplastic polyurethane honeycombs with graded densities. The results indicate that the ability of density grading of TPU structures to afford excellent impact protection in harsh environmental conditions. Yu et al. [17] showed that the graded Schwarz P structure fabricated by additive manufacturing has a great capacity of absorption energy during the compression experiment, while energy absorbed in the graded Gyroid structure was close to the uniform Gyroid structure. Pajunen et al. [18] performed an experimental investigation to compare the response characteristics of a 3D-printable structure with a pin-jointed tensegrity structure. Research paves the way for new research in the area of manufacturable tensegrity-

inspired metamaterials. Kuciewicz et al. [19–21] developed a new procedure for studying the mechanical performance of a regular cellular structure fabricated by fused deposition modelling of ABSplus material under static loading conditions. The same authors utilized a new technique for damage modeling of a regular cellular structure manufac-

Mechanical properties of CF-PEKK.

Density ASTM D792 1.27 g/cm³

Tensile Modulus ASTM D638 2.9 GPa

Flexural Modulus ASTM D790 3 GPa

Elongation at break ASTM D638 >80%

Impact IZOD ASTM D256 5.5 kJ/m²

tured by additive manufacturing. On the other hand, Keshavarzan et al. [22] investigated the damage mechanism of triply periodic minimal surface cellular structures under compressive loadings fabricated by Vat photopolymerization additive manufacturing. The results indicated that the principal damage mechanism is the formation of primary and secondary shear bands. In another work, Nazir et al. [23] carried a numerical simulation and an experimental investigation to understand the buckling behavior of additively manufactured cellular columns. It was found that the critical buckling load rises with the rise of unit cell size or diminish of cellular column height.

Many of the research work investigated experimentally the dynamic behaviour and fatigue damage of composite materials fabricated by conventional techniques under impact loading [24–29]. In additions, several empirical relations were established to characterize the repeated impact of materials. Repeated impact behavior is generally characterized by various parameters such as the impact velocity, the maximum stress amplitude in the impact, the loading time and the absorbed energy [30,31]. To date, any characterization of repeating impact has to be based on an understanding of the process in a single (standard) impact. Also, there are not a lot of researches regarding the investigation of the dynamic behavior of the honeycombs structures fabricated by additive manufacturing. In this study, the authors studied the dynamic behaviour of a honeycomb structure for different filling densities (20%, 50% and 100%) employed the SHPB considering different impact pressure. On the other hand, samples have

been submitted to repeated dynamic compression cycles using the SHPB method. The obtained results proved that the cyclic dynamic loading drastically changed the dynamic behavior of the material compared to standard dynamic loading.

1. Materials and structural design

2.1. Materials

In this work, the composite (CF-PEKK) was selected as material which has an excellent mechanical performance[32]. This material is considered an advanced engineering polymer, which belongs to the PAEK family, mixed with carbonfibre. The CF-PEKK stands out when gathering high values of resistance in all fields. The Young Module (Traction Module) of the PEKK CF (2900 MPa) is superior to that of the technical materials of 3D printing by more than 30%; Nylon-



Fig. 1. Fused filament fabrication (FFF) process.

Carbon Fibre CF15 (500 MPa), PC-Max (2048 MPa), Nylon PolyMide COPA (2223 MPa). The Flex Module of the PEKK CF is 3000 MPa, again surpassing all conventional and technical 3D printing materials, Nylon PolyMide COPA (1667 MPa), ABS Premium (2000 MPa), PC- Max (2044 MPa). This material has produced by NANOVIÀ from France. The mechanical properties CF-PEKK stands out after having achieved high resistance values in all fields (See Table 1).

2.2. Structural design

The specimens illustrated in this research were fabricated by the FFF process. The scheme of the FFF system operation and the 3D printing system of the large French manufacturer NANOVIÀ used in our

Table 2

Parameters of Fused Filament Fabrication (FFF) processing.

Extrusion temperature 380 °C

Heat platform temperature 100 °C

Nozzle 0.3 mm

Nozzle moving speed 20 mm/s first layer 40 mm/s other layers Diameter
1.75/2.85 mm \pm 50 μ m Moisture absorption 0.2%

study for the printing of specimens are presented in Fig. 1. The characteristics of the printing of all samples are listed in Table 2.

An experimental investigation was conducted on three configurations of CF-PEKK composites. Specimens of length 12.9 mm, an exterior diameter 16.8 mm and 15 mm inner diameter are fabricated using the FFF process. To understand the mechanical properties the infill density is varied while fabricating the specimens. The specimens were designed in CATIA was converted the data into STL file through SLIC3R. Finally, after the slicing processing, it is saved in G-format. G-code file was fed into the 3D printing machine controller. All samples employed to test the effect of the filling density were fabricated with the same filling pattern-honeycomb, with the filling density 20%, 50% and 100% respectively as illustrated in Fig. 2.

As explained previously, the filling should be chosen according to the specific needs of each print job. The main reason for printing less than 100% of the filling piece is to decrease the costs and printing time. Table 3 shows the number of parts printed and the comparison between the

differentfilling densities in terms of printing time and the amount of material required.

1. Test machine

The experimental test employed in this present work is the SHPB, which is a typical test to assess the dynamic behaviour of the material under high strain rates (200 and 10⁴ s⁻¹) [24-27]. This system aimed



Fig. 2. Three configurations of short carbon—fibre-reinforced PEKK composites.

Table 3

Details of the 3D printing of the tested parts.

Infill densities	Number of specimens	Number of layers	Total number of lines	Filament required (mm)	Extruder 1 (mm)	Printing time
20%	40	43	428,161	12,183	12,183	8h21mn37s
50%	40	43	496,561	18,954	15,913	12h48mn59s
100%	40	43	812,628	21,306	21,306	15h04mn53s



Fig. 3. Schematic representation of the experimental procedure.



Fig. 4. Reproducibility of tests, $P = 1.4$ bar.

to make a given impact pressure to the specimen located between two bars incident and transmitted in order to analyze its dynamic response at a given strain rate. The characteristics of the SHPB system are the incident, transmitted and impactor bars. The impactor bar of 0.5 m length and a diameter 20 mm. Both the incident and transmitted bars had a length of 1.9850 m and a diameter of 20 mm. Three pulses $\epsilon_I(t)$, $\epsilon_R(t)$ and $\epsilon_T(t)$ respectively incident, reflected and transmitted strain were measured by the strain gauges and amplified by a dynamic strain indicator mounted at the middle of each bar, and then recorded by a digital oscilloscope (see Fig. 3). The signals are treated with Maple Software package using fast Fourier transformation to obtain the evolution of the dynamic parameters: stress vs. strain, strain rate vs. time, incident and transmitted load and velocity at the interfaces input bar/

PEKK in the SHPB tests. The applied frame rate was 30,000 fps (frames per second). The camera was triggered by the incident wave signal using the 'start' trigger mode.

The specimens were subjected to various impact pressures, and the resulting signals were registered by a digital oscilloscope. Utilizing the data registered by the strain gauges, the displacements of the bar interfaces are given by [33-35]:

t

$$\frac{1}{2} \left(\frac{\partial \epsilon_I}{\partial t} + \frac{\partial \epsilon_R}{\partial t} \right) = \frac{\partial \epsilon_T}{\partial t}$$

0

$$u(t) = C \int_0^t \ddot{u}(\tau) d\tau$$

$$\ddot{u}_2 \approx \frac{1}{4}$$

0

$$\varepsilon_T \approx \frac{1}{2}$$

$$\ddot{u}_2 \approx \frac{1}{4}$$

0

sample and output bar/sample vs. time. The Photron FASTCAM high-speed video camera was used to track the deformation process of CF-

where the interval $[0, t]$ cover the first cycle (incident-reflected- transmitted signal). $u_1 \ddot{u}_1$, $u_2 \ddot{u}_2$, $\varepsilon_I \ddot{\varepsilon}_I$, $\varepsilon_R \ddot{\varepsilon}_R$ and $\varepsilon_T \ddot{\varepsilon}_T$ denote the dis-



placement of the incident bar interface, displacement of the transmitted bar interface, incident, reflected and transmitted pulses, respectively. Therefore we deduce the relative displacement between the two bars interfaces (or elongation).

$$Z$$

$$Z$$

$$t$$

$$\frac{\partial u}{\partial t} \approx u_1 - u_2 \approx C_0 \frac{\partial \epsilon_I}{\partial t} - \epsilon_R \approx C_0 \frac{\partial \epsilon_T}{\partial t} \quad (3)$$

0

0

where the velocity of the strain wave C_0 is given by:

$$\frac{\partial \epsilon}{\partial t} \approx \frac{1}{L} \frac{\partial \epsilon_R}{\partial t} \quad (4)$$

ρ

$$2c_0$$

$$\epsilon_{-} \approx \frac{1}{L} \int \epsilon_R dt \quad (5)$$

where L is the original gauge length of the specimen, $\epsilon_r(t)$ is the time-resolved strain associated with the reflected wave in the incident bar (IB), and c_0 is the elastic wave velocity of the bar material. The following basic relations are hence used to determine the dynamic properties (strain $\epsilon(t)$, stress $\sigma(t)$, loads $F(t)$ and velocities $V(t)$) of the material at the given strain rates: $2c_0 \int \epsilon dt \approx L$

$$\epsilon_r \approx \frac{\partial \epsilon}{\partial t} \quad (6)$$

$$A_s$$

0

where E and ρ are the modulus and the density of the bar, respectively. However, The nominal strain rate can be determined by considering a homogeneous deformation of the specimen respecting to one-

dimensional wave theory, as:

$$\sigma(t) = A_t E_t \epsilon_t(t) \quad (7)$$



where A_s is the cross-sectional area of the specimen, and $\epsilon_t(t)$ is the time-resolved axial strain in the transmission bar (TB) of cross-sectional area A_t and Young's modulus E_t .

$$F_i(t) = A_b E_b \epsilon_i(t) - \epsilon_r(t) \quad (8)$$

$$F_t(t) = A_b E_b \epsilon_t(t) \quad (9)$$

$$V_i(t) = -C_0 \epsilon_i(t) - \epsilon_r(t) \quad (10)$$

$$V_t(t) = C_0 \epsilon_t(t) \quad (11)$$

1.

Experimental results

4.1. Test reproducibility for different impact pressure

Before conducting the dynamic compression tests with Hopkinson bars, it is important to assure the repeatability of dynamic tests [36,37]. In this context, all samples were tested three times for different impact pressures with the same intensity of the incident wave to verify reproducibility. Both the incident and reflected waves are obtained for the different filling density

of CF-PEKK ranging from 20% to 100%. The representative repeatable strain vs time variation for filling density of CF/PEKK is presented in Fig. 4.



Fig. 7. Dynamic behaviour, CF-PEKK at 2 bar.

4.2. Dynamic behaviour

This section presents the experimental results of the compression tests carried out on the SHPB apparatus for different infill densities. Figs. 5–8 show the different dynamic parameters. From these figures, it's clear that the different dynamic parameters increase with increasing impact pressure. It can be seen also that all specimens exhibit similar compressive behaviour for the three infill densities (20%, 50% and 100%) at different impact pressures. On the other hand, it can be remarked that the transmitted signal is generally weak, but it is very weak for low filling rates. Also, it can be seen that the reflected signal is of the same order as the incident signal (Fig. 5). This can be considered as a strong indicator of the capacity of the material to attenuate/ absorb dynamic loads. So, it can be remarked that all experiments correspond to the non-damaged case because the pressure wave is

reflected through the printed samples with an honestly elastic response. On the other hand, the strain rate rises quickly under achieving a peak value which is proportionally depended to the impact pressure. Then, it diminishes and thereafter tends to go down to zero for the various impact pressure. For all impact pressures, it's can be seen that the strain rate achieves negative values, which correspond to elastic springback of the specimens. It's confirmed that all tests correspond to non-damaged tests for different infill density. Concerning the load's curves, it has been first shown that these curves at both ends of the sample were equilibrated which satisfies the basic assumption for a valid SHPB experiment.

In the curves of stress–strain, it's can be remarked that the dynamic behaviour of the CF-PEKK is highly influenced by the strain rate. At the macroscopic scale, the classical behaviour (in terms of stress–strain) of a honeycomb structure under compressive loading is characterized by



Fig. 8. Dynamic behaviour, CF-PEKK at 2.4 bar.

three phases; an elastic phase limited by threshold stress followed by a stress plateau (abusively called a plastic plateau) and an ultimate phase densification during which the stress rises strongly as a function of the deformation. This behaviour of the honeycomb structure under compression is classical; it has been presented by many authors [38,39].

The typical compressive stress–strain behaviour of an elastic cellular structure shows three main regimes: an initial linear elastic regime, where the strain energy is stored in the reversible bending of the struts, a plateau regime, where small increases in load lead to very large additional strain, and finally a densification regime where struts begin to impinge upon each other. At this last stage, the cellular material starts to exhibit a modulus approaching that of the solid material from which it is made. On the other hand, It is important to note that there exists given energy for any cellular structure to which it is optimally suited to absorb; this is the energy that compresses the structure to the point just before densification, at the end of the stress plateau. Larger compression energies will densify the structure, transferring high stresses and lower compression energies could be more efficiently absorbed by a lower density structure. A schematic of the typical stress–strain curve is shown in Fig. 9.

In our case, taking the stress–strain response at 2.4 bar as an exam— ple, it is noteworthy that the mechanical responses illustrate good repeatability among all the compression tests. Like most of the other cellular structure [38], the stress–strain curves of 3D printed CF- PEKK subjected to high strain rate compression can be identified by the three regions (refer to Fig. 10):

A) an initial, approximately linear elastic stage is followed by a peak which represents the fracture resistance of the developed 3D printed CF-PEKK; B) the drop in stress and the long plateau stage (crushing) with a nearly constant stress form the second region which determines the energy absorption capacity of the structure; and C) the last densification region is characterized by the dramatical stress increase when the strain.


To understand the deformation process of the CF-PEKK composite under dynamic loading, a high-speed camera is employed to record the loading of the specimen. Fig. 11 shows the compression deformation process for three infill densities structures at 2.4 bar. The main deformation modes observed for the three infill density are crushing and local buckling without any macroscopic damage. The on-line observation in the dynamic test reveals that buckling occurs in the places where the cell wall direction is approximately parallel to the 

Fig. 9. Typical compressive stress–strain curve of a cellular structure [40].



Fig. 10. Stress–strain response at 2.4 bar.

loading direction. The occurrence of this buckling phenomenon contributes to a noticeable drop in stress.

To clearly shows the temporal variation of the stress according to the strain rate. Four characteristic zones could be defined as shown in Fig. 12:

- Zone 1: Rapid rise of strain rate values, which could be traduced by the self-fixation of the sample between the incident and transmitted bars. •

- Zone 2: Dynamic strength created a diminution in strain rate and a rise in stress after reaching a flawless connection between the bars

and the sample.

- Zone 3: For the standard and the first dynamic compression cycles, one can see that when reaching a maximum value, the stress started to increase

significantly with the presence of several oscillations

however the strain rate tended to decrease progressively. For the case of the 2nd and 3rd cycles, the 3rd zone was characterized by quasi-stabilization of strain rates profile at maximum values which increased with the number of the dynamic compression cycle.

- Zone 4: In the 4th zone of each dynamic compression cycle, the

impacted sample became more solid, which generated a sudden decrease in strain rate. In this region, one can see that stress always decreased but at a much slower rate than the strain rate.

4.3. Repeated impact response

The obtained dynamic (incident, reflected and transmitted) raw signals at each dynamic compression cycle using SHPB were shown



Fig. 11. High-speed photographs of the dynamic deformation process for three infill density at 2.4 bar.



Fig. 12. Variation of stress and strain rate during dynamic compression at 2.4 bar.

in Fig. 13. As shown in this Figure, the incident pulses registered on the incident bar for specimens at different repeated dynamic compression were almost the same due to the same impact pressure (2,4 bars) produced by the sticker bar at each dynamic compression test. However, one can note that the reflected and transmitted pulses were significantly affected by the repeated dynamic loading because of the rise in the strain rate with the number of dynamic compression tests and the state of the material evolves with each test.

It is observed that the repeated dynamic loading had a significant effect on the dynamic response. From the test results, the following conclusions were made: (1) the sample stiffness and the maximum stress rise meaningfully with the number of dynamic compression loading because the impacted specimen became more solid, which generated a sudden decrease in strain rate; (2) the incident and transmitted load and only the transmitted velocity amplitude augmented with the augmentation in the number of tests. However, the incident velocity increased considerably when the number of tests increased. The reason for this phenomenon was that at the standard dynamic compression test, the material had no much damage and thus the dynamic compressive wave could propagate quickly in the whole of the sample. However, when the number of tests increased the dynamic compression wave had much time to propagate into all the discontinuous sublaminae of the laminate. Fig. 14 shows the variation of the strain rate vs impact pressure for three infill density. From this Figure, it can be noted that the specimens manufactured with a 100% infill density had the highest resistance in compression experiment. The strain rate of samples with a 20%–50% infill density augmented meaningfully. This relationship is almost linear; the peak dynamic stress and maximum strain (%) is proportional to the infill density at different impact pressures. This result indicates that the infill density has a great effect on the modulus of elasticity of the CF-PEKK samples.



Fig. 13. Repeated dynamic loading of CF-PEKK (100%) at 2.4 bar.



Fig. 14. Strain rate vs. Impact pressure.

1.
Conclusion

This research work has analysed the influence of varying the infill density on the dynamic behaviour of the 3D printed of CF-PEKK specimens. The cylindrical CF-PEKK printed specimens were subjected to dynamic loading using the SHPB apparatus. The characteristics of the SHPB were determined according to impact pressure for the three infill density (20%, 50% and 100%). In the other hand, the dynamic behavior of 3D printed of CF-PEKK submitted to repeated impact using SHPB had been examined in this paper and it was concluded that the impact-fatigue was considered as a critical form of loading. Experimental results show that the increase infilling density reduces deformation and the mechanical strength of the sample increases. Low infill densities are recommended for quick printing but not mechanical strength (20%). However, this analysis showed that the damage modes generated in repeated impact cycles were different from those in standard dynamic compression loading without pre-impact. From this research, it was found that printing solid infill is beneficial in the case

of dynamic compression specimen when compared to non-solid infill patterns. Low infill densities are recommended for quick printing but not mechanical strength. The main reason for printing less than 100% of the filling piece is to diminish the printing time and costs as long as the strength of the partial filling sample does not deteriorate drastically compared to that of the solid parts. The research presented in this article is a part of on-going work and our future research imply quantifying the absorption energy on impact and developing a numerical model to correlate with the experimental results. Followed by a parametric study to understanding the effect of printing orientation, density, and filler pattern on the compressive performance.

CRediT authorship contribution statement M. Nachtane: Investigation, Methodology, Data curation, Conceptualization, Writing-original draft, Writing-review & editing. M. Tarfaoui: Investigation, Conceptualization, Methodology, Supervision, Project administration, Software, Resources, Writing-review & editing. Y. Ledoux: Writing -original draft, Validation. S. Khammassi: Investigation. E. Leneveu: Resources, Validation, Funding acquisition.

J. Pelleter: Resources, Validation, Funding acquisition.

Declaration of Competing Interest The authors declare that they have no known competing financial interests or personal relationships that could have appeared to influence the work reported in this paper.

References

- [1] [Zahlan N, O'Neill JM. Design and fabrication of composite components; the spring- forward phenomenon. Composites 1989;20\(1\):77–81.](#) [2] [El Moumen A, Tarfaoui M, Lafdi K. Additive manufacturing of polymer composites: Processing and modeling approaches. Compos B Eng 2019;171:166–82.](#) [3] [Yang L, Harrysson O, West H, Cormier D. Mechanical properties of 3D re-entrant honeycomb auxetic structures realized via additive manufacturing. Int J Solids Struct 2015;69:475–90.](#) [4] [Ganghoffer JF, Goda I, Novotny AA, Rahouadj R, Sokolowski J. Homogenized couple stress model of optimal auxetic microstructures computed by topology optimization. ZAMM-J Appl Math Mech/Z Angew Math Mech 2018;98 \(5\):696–717.](#)
- [5] [Goda I, Dos Reis F, Ganghoffer JF. Limit analysis of lattices based on the asymptotic homogenization method and prediction of size effects in bone plastic collapse. In Generalized Continua as Models for Classical and Advanced Materials. Cham: Springer; 2016. p. 179–211.](#)
- [6] [Goda I, Rahouadj R, Ganghoffer JF. Size dependent static and dynamic behavior of trabecular bone based on micromechanical models of the trabecular architecture. Int J Eng Sci 2013;72:53–77.](#)
- [7] [Goda I, Ganghoffer JF. 3D plastic collapse and brittle fracture surface models of trabecular bone from asymptotic homogenization method. Int J Eng Sci 2015;87:58–82.](#) [8] [Rybachuk M, Mauger CA, Fiedler T, Öchsner A. Anisotropic mechanical properties](#)

[of fused deposition modeled parts fabricated by using acrylonitrile butadiene styrene polymer. J Polym Eng 2017;37\(7\):699–706.](#)

[9] [Xiao J, Gao Y. The manufacture of 3D printing of medical grade TPU. Prog Add Manuf 2017;2\(3\):117–23.](#) [10] [Fadida R, Rittel D, Shirizly A. Dynamic mechanical behavior of additively manufactured Ti6Al4V with controlled voids. JAppl Mech 2015;82\(4\).](#) [11] [Tsouknidas A, Pantazopoulos M, Katsoulis I, Fasnakis D, Maropoulos S, Michailidis](#)

[N. Impact absorption capacity of 3D-printed components fabricated by fused deposition modelling. Mater Des 2016;102:41–4.](#)

[12] [Fernandez-Vicente M, Calle W, Ferrandiz S, Conejero A. Effect of infill parameters on tensile mechanical behavior in desktop 3D printing. 3D Print Addit Manuf 2016;3\(3\):183–92.](#) [13] [Wyatt H, Safar A, Clarke A, Evans SL, Mihai LA. Nonlinear scaling effects in the](#)

[stiffness of soft cellular structures. R Soc Open Sci 2019;6\(1\):181361.](#)

[14] [Zhang P, Arceneaux DJ, Khattab A. Mechanical properties of 3D printed polycaprolactone honeycomb structure. J Appl Polym Sci 2018;135\(12\):46018.](#) [15] [Antolak-Dudka A, Płatek P, Durejko T, Baranowski P, Małachowski J, Sarzyński M,](#)

[et al. Static and Dynamic Loading Behavior of Ti6Al4V Honeycomb Structures Manufactured by Laser Engineered Net Shaping \(LENSTM\) Technology. Materials 2019;12\(8\):1225.](#)

[16] [Bates SR, Farrow IR, Trask RS. Compressive behaviour of 3D printed thermoplastic polyurethane honeycombs with graded densities. Mater Des 2019;162:130–42.](#) [17] [Yu S, Sun J, Bai J. Investigation of functionally graded TPMS structures fabricated by additive manufacturing. Mater Des 2019;182:108021.](#) [18] [Pajunen K, Johannis P, Pal RK, RimoliJJ, Daraio C. Design and impact response of 3D-printable tensegrity-inspired structures. Mater Des 2019;182:107966.](#) [19] [Kucewicz M, Baranowski P, Stankiewicz M, Konarzewski M, Płatek P, MałachowskiJ. Modelling and testing of 3D printed cellular structures under quasi-static and dynamic conditions. Thin-](#)

[Walled Struct 2019;145:106385](#). [20] [Kucewicz M, Baranowski P, Małachowski J, Popławski A, Płatek P. Modelling, and characterization of 3D printed cellular structures. Mater Des 2018;142:177–89](#). [21] [Kucewicz M, Baranowski P, Małachowski J. A method of failure modeling for 3D printed cellular structures. Mater Des 2019;174:107802](#).

[22] [Keshavarzan M, Kadkhodaei M, Badrossamay M, Ravari MK. Investigation on the failure mechanism of triply periodic minimal surface cellular structures fabricated by Vat photopolymerization Additive Manufacturing under compressive loadings. Mech Mater 2020;140:103150](#). [23] [Nazir A, Jeng JY. Buckling behavior of additively manufactured cellular columns: Experimental and simulation validation. Mater Des 2020;186:108349](#). [24] [Gemi L, Kara M, Avci A. Low velocity impact response of prestressed functionally graded hybrid pipes. Compos B Eng 2016;106:154–63](#). [25] [Gemi L. Investigation of the effect of stacking sequence on low velocity impact response and damage formation in hybrid composite pipes under internal pressure. A comparative study. Compos B Eng 2018;153:217–32](#). [26] [Hassoon OH, Tarfaoui M, El Moumen A, Benyahia H, Nachtane M. Numerical](#)

[evaluation of dynamic response for flexible composite structures under slamming impact for naval applications. Appl Compos Mater 2018;25\(3\):689–706](#).

[27] [Gemi L, Köroğlu MA, Ashour A. Experimental study on compressive behavior and](#)

[failure analysis of composite concrete confined by glass/epoxy±55 filament wound pipes. Compos Struct 2018;187:157–68](#).

[28] [Nachtane M, Tarfaoui M, El Moumen A, Saifaoui D. Numerical investigation of](#)

[damage progressive in composite tidal turbine for renewable marine energy. In: 2016 International Renewable and Sustainable Energy Conference \(IRSEC\). IEEE;](#)

[2016. p. 559–63.](#)

[29] [Gemi L, Kayrı M, Uludağ M, Gemi DS, Şahin ÖS. Experimental and statistical analysis of low velocity impact response of filament wound composite pipes. Compos B Eng 2018;149:38–48.](#)

[Compos B Eng 2018;149:38–48.](#)

[30] [Roy R, Sarkar BK, Bose NR. Impact fatigue of glass fibre–vinylester resin composites. Compos A Appl Sci Manuf 2001;32\(6\):871–6.](#) [31] [Ding YQ, Yan YBAUOU, McIlhagger RBAUOU. Effect of impact and fatigue loads on the strength of plain weave carbon-epoxy composites. J Mater Process Technol, 1995; 55\(2\): 58–62.](#) [32] [Donadei V, Lionetto F, Wielandt M, Offringa A, Maffezzoli A. Effects of Blank](#)

[Quality on Press-Formed PEKK/Carbon Composite Parts. Materials 2018;11 \(7\):1063.](#)

[33] [Tarfaoui M, Nachtane M. Can a three-dimensional composite really provide better mechanical performance compared to two-dimensional composite under compressive loading? J Reinf Plast Compos 2019;38\(2\):49–61.](#) [34] [Tarfaoui M, Nachtane M, El Moumen A. Energy dissipation of stitched and](#)

[unstitched woven composite materials during dynamic compression test. Compos B Eng 2019;167:487–96.](#)

[35] [El Moumen A, Tarfaoui M, Nachtane M, Lafdi K. Carbon nanotubes as a player to improve mechanical shock wave absorption. Compos B Eng 2019;164:67–71.](#) [36] [Sassi S, Tarfaoui M, Nachtane M, Yahia HB. Strain rate effects on the dynamic compressive response and the failure behavior of polyester matrix. Compos B Eng 2019;174:107040.](#) [37] [Nachtane M, Tarfaoui M, Sassi S, El Moumen A, Saifaoui D. An investigation of hygrothermal aging effects on high strain rate behaviour of adhesively bonded composite joints. Compos B Eng 2019;172:111–20.](#) [38] [Bouix Rémy, Viot Philippe, Lataillade Jean-Luc. Polypropylene foam behaviour](#)

under dynamic loadings: Strain rate, density and microstructure effects. IntJ Impact Eng 2009;36(2):329–42.

[39] Li D, Liao W, Dai N, Xie YM. Comparison of mechanical properties and energy absorption of sheet-based and strut-based gyroid cellular structures with graded densities. Materials 2019;12(13):2183. [40] Goga V. Measurement of the energy absorption capability of polyurethane foam. Bratislava, Slovak Republic: University of Technology Faculty of Electrical Engineering and Information Technology; 2010. Retrieved October, 28, 2016.